Journal of the Geological Society, London, Vol. **170**, 2013, pp. 557–570. doi: 10.1144/jgs2012-016
Published *Online First* on April 22, 2013

Open-system processes in the differentiation of mafic magma in the Teide–Pico Viejo succession, Tenerife

SEBASTIAN WIESMAIER[1,2], VALENTIN R. TROLL[2,3], JOHN A. WOLFF[4] & JUAN CARLOS CARRACEDO[2]

[1]*Ludwig-Maximilians-Universität München, Department of Earth and Environmental Sciences, 80333 München, Germany*
[2]*Department of Physics (Geology), GEOVOL, University of Las Palmas, Gran Canaria, Spain*
[3]*Uppsala University, Department of Earth Sciences, CEMPEG, Villavägen 16, 75236 Uppsala, Sweden*
[4]*Washington State University, Department of Geology, Washington State University, Pullman 99164, WA, USA*
**Corresponding author (e-mail: sebastian.wiesmaier@min.uni-muenchen.de)*

Abstract: Oceanic island basalts are commonly thought to differentiate by fractional crystallization, yet closed-system fractionation models have so far failed to reproduce major and trace element variations observed in mafic lavas from the Teide–Pico Viejo stratovolcano complex on Tenerife. Here, new high-precision plagioclase trace element data are fed into such a fractionation model. The results confirm that fractionation of phenocrysts found in the lavas does not reproduce trace element variations, in particular enrichment of Sr and Zr observed in the Teide–Pico Viejo mafic suite. This enrichment of Sr and Zr is tested by an energy-constrained recharge, assimilation and fractional crystallization (EC-RAFC) model at high T and low ΔT intervals, consistent with previously determined magma storage beneath Tenerife at sub-Moho depths. Published mineral–melt equilibrium relations using the plagioclase anorthite content ($0.4 < X_{An} < 0.8$) constrain the temperature during differentiation. Gabbroic xenoliths found in Tenerife lavas are assumed as contaminant. Enrichment of Sr and Zr in the Teide mafic suite is reproduced by this combined assimilation and fractional crystallization model, as assimilation causes higher degrees of enrichment in incompatible trace elements than is possible by crystal fractionation alone. Recycling of plutonic roots may thus have significantly enriched trace elements in the primitive lavas of the Teide–Pico Viejo succession.

Supplementary material: Detailed average mineral compositions of low and high Sr–Zr lavas, composition of the bulk extracts and full graphs of the recalculated closed-system model are available at www.geolsoc.org.uk/SUP18604.

The role of open-system processes in the petrogenesis of ocean-island volcanic suites has been controversial (Davidson & Bohrson 1998). The fundamental problem is the compositional similarity of ocean-island crust and mantle-derived basaltic magma; consequently, signs of crustal assimilation are subtle and hard to detect. The Teide–Pico Viejo succession in Tenerife, Canary Islands contains abundant mafic lavas with compositions that are in disequilibrium with mantle olivine. This implies pre-eruptive differentiation of mafic magmas, which has been modelled by closed-system fractional crystallization (Ablay *et al.* 1998). Up to now, the Teide–Pico Viejo complex has mainly been studied as a prime example for the formation of felsic magma in ocean islands (Ridley 1970; Araña *et al.* 1989; Albert-Beltrán *et al.* 1990; Ablay *et al.* 1998; Carracedo *et al.* 2007; Wiesmaier *et al.* 2012). Recently, the radiogenic isotope signatures of the basanite–phonolite sequence at Teide have been found to be strongly affected by open-system processes, including assimilation of pre-Teide island core material (Wiesmaier *et al.* 2012). This invites the question of whether more mafic magmas at Teide–Pico Viejo are also the products of assimilation and magma mixing. However, the radiogenic isotope ratios of basanites in this sequence are essentially uniform or mirror the assumed mantle compositions. As a result, analyses of radiogenic isotopes are insufficient for constraining the differentiation processes that gave rise to Teide–Pico Viejo mafic compositions. The focus of this study is therefore to compare open- and closed-system models based on major and trace element concentrations, including appropriate compositions for a potential contaminant.

This revision of the previous model of differentiation is based on three factors. First of all, high-precision plagioclase trace element data from the Teide–Pico Viejo succession are now available (Wiesmaier 2010). These data allow refinement of the closed-system model presented for Teide by Ablay *et al.* (1998). For example, in mafic liquids, plagioclase is the main phase that incorporates Sr. This trace element may thus serve as a tracer of magmatic differentiation in Teide mafic lavas, which previously could not be determined owing to lack of *in situ* trace element data. Furthermore, the calculated bulk partition coefficients for Sr are now more reliable, because they are based on measured *in situ* data.

Second, empirical equations on the relationship of anorthite content in plagioclase and temperature of crystallization allow the thermal conditions in a magma reservoir during crystallization of plagioclase to be constrained (e.g. Blundy & Wood 1991; Bindeman *et al.* 1998; Bindeman & Bailey 1999; Bédard 2006; Namur *et al.* 2012). The wide stability field of feldspar (equivalent to 0–25 km depth in the crust; Borghini *et al.* 2009, and references therein), its ability to crystallize from a wide variety of melt compositions and its sustained 'resistance' to diffusional re-equilibration of major elements (e.g. Morse 1984) imply that plagioclase data are a robust means of reconstruction of some of the intensive parameters that affected crystallization (see Namur *et al.* 2012, and references therein).

Finally, an energy-constrained recharge, assimilation and fractional crystallization (EC-RAFC) model (Spera & Bohrson 2001) is calculated to investigate the thermal and compositional evolution

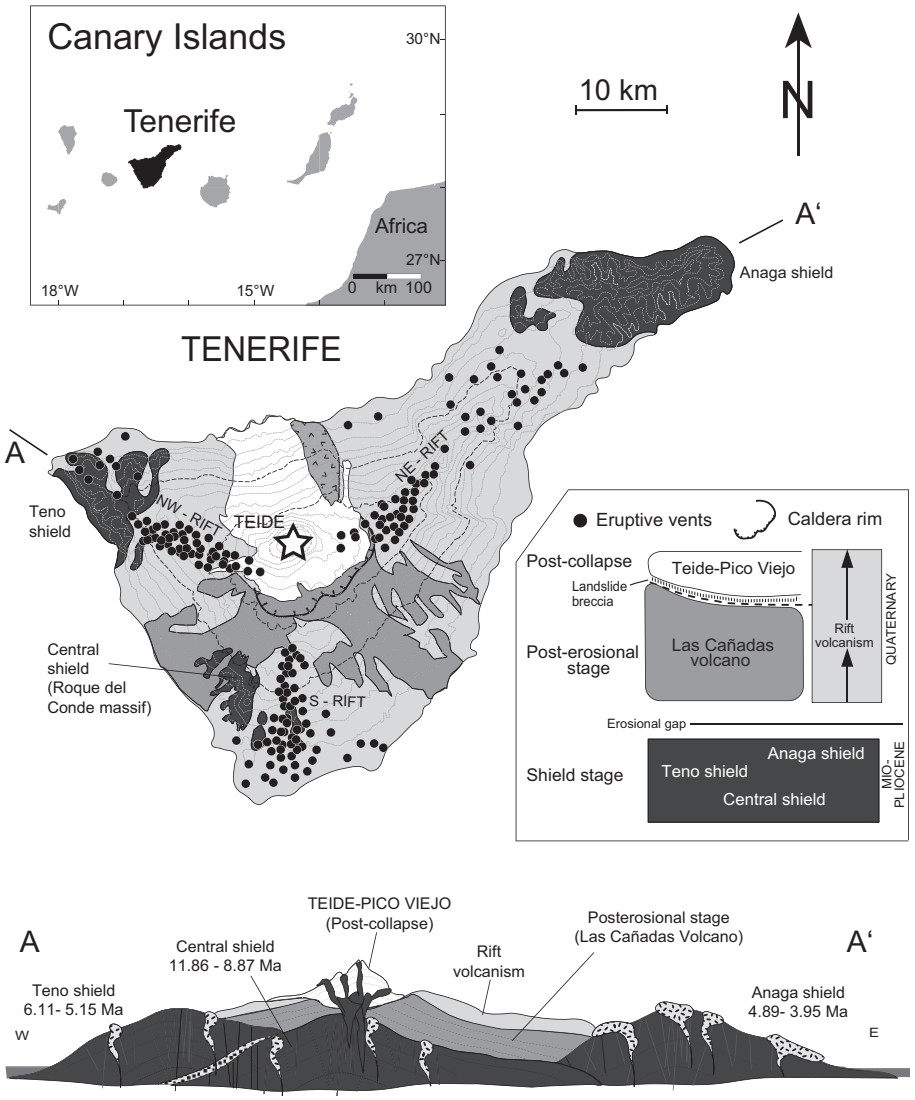

Fig. 1. Simplified geological map of Tenerife modified from Carracedo *et al.* (2007). The three overlapping shield volcanoes Roque del Conde, Teno and Anaga (white) constitute the mafic foundation of the island and are centrally overlain by the mafic to felsic Las Cañadas volcano (light grey). Dark grey indicates lava flows emanated from three rift zones to the NW, NE and south (black dots represent the vent distribution in the rift zones). The rift zone activity is intercalated with Las Cañadas volcano and simultaneous with Teide–Pico Viejo (see simplified stratigraphic column). Black shading represents the most recent succession in Tenerife, Teide–Pico Viejo, nested inside the Las Cañadas–Icod collapse embayment that incised Las Cañadas volcano at *c*. 200 ka.

of Tenerife mafic magma at depth. The new plagioclase data, along with the revised bulk partition coefficients, and the thermal constraints from the empirical equations on anorthite content are fed into the EC-RAFC model. This combination of thermodynamic and compositional parameters embedded in a framework of realistic thermal conditions ensures a rigorous approach to evaluating whether or not open-system processes may be at work in the petrogenesis of mafic lavas of the Teide–Pico Viejo sequence.

This study therefore focuses on lavas of the Teide–Pico Viejo succession with SiO_2 <53 wt%. First, the closed-system model is tested by updating the approach of Ablay *et al.* (1998) with new high-precision microanalytical data from a large number of plagioclase crystals for their major and trace element compositions (Wiesmaier 2010) and whole-rock major and trace element data from Rodríguez-Badiola *et al.* (2006). Then, the temperature of plagioclase crystallization is reversely modelled using the empirical relationships from the literature. Finally, plagioclase data, bulk partition coefficients derived from the closed-system model and temperature information are fed into an EC-RAFC model to test for a combination of assimilation and magma mixing during continuing fractional crystallization.

Geology of Tenerife

The overall structure of Tenerife is controlled by a three-armed rift zone system (Fig. 1). The three arms to the NW, NE and south join beneath Teide–Pico Viejo volcano. Proto-rifts may have already been active as early as Miocene times (Carracedo *et al.* 2011). The NW and NE arms of this system are volcanically active and extend into the peripheral shield volcanoes Teno and Anaga (Carracedo 1994). The rifts show mainly mafic volcanism (basanite to phonotephrite) originating from single or multiple (and often aligned) monogenetic cones. Mineral assemblages are restricted to olivine, augite, Fe–Ti oxides and in some cases plagioclase.

Prior to the formation of the central Teide complex, a giant landslide incised the central Las Cañadas volcano complex at *c*. 200–180 ka, at the junction of the three rift zones, to leave behind the Icod collapse scar (Watts & Masson 1995; Carracedo 1999; Carracedo *et al.* 2007; Márquez *et al.* 2008). Pre-existing vertical collapse structures probably contributed to the lateral instability of Las Cañadas volcano (e.g. Martí *et al.* 1994, 1997; Troll *et al.* 2002). The Icod landslide unroofed the triple junction of the rift zone (see Márquez *et al.* 2008) and initiated the construction of proto-Teide inside this collapse embayment.

The Teide–Pico Viejo succession is the youngest eruptive sequence of Tenerife and consists of the central Teide–Pico Viejo complex, the monogenetic vents located around Teide–Pico Viejo, and vents of the NW and NE rift zones that are contemporaneous with the Teide–Pico Viejo complex (Carracedo *et al*. 2007).

Initial eruptions at Teide–Pico Viejo produced mafic lavas indistinguishable from rift zone eruptions (Carracedo *et al.* 2007). Between 30 and 20 ka, the Teide–Pico Viejo edifice and its flank vents began to erupt more differentiated material, producing exclusively phonolite during the last 20 kyr (Carracedo *et al.* 2007). The phonolites show significant contamination by a radiogenic Sr island edifice component, most probably at shallow depths (Wiesmaier *et al*. 2012) . This evolution probably resulted from the establishment of a shallow magmatic plumbing system underneath the progressively growing central complex. The rift zones continued to erupt mafic compositions, sampling deeper sub-Moho to intermediate oceanic crust reservoirs. The interaction between these two regimes, rift zone and central volcano, is shown in the boundary zone between them, where mixing of rift zone basanite and central complex phonolite magmas has occurred (Araña *et al.* 1994; Wiesmaier *et al.* 2011). This study exclusively focuses on the mafic lavas erupted in the Teide–Pico Viejo succession. The samples therefore comprise rocks from the initial eruptions of Teide–Pico Viejo along with a large number of samples from the currently active rift zones.

Previous work on the Teide–Pico Viejo succession

The closed-system model of Ablay et al. (1998)

Ablay *et al.* (1998) proposed a model of closed-system fractional crystallization for Teide–Pico Viejo lavas on the basis of analysed major element mineral compositions and a multiple-step mass-balance calculation with a least-squares regression analysis for every modelled step. Trace elements were modelled using whole-rock concentrations and partition coefficients from the literature. *In situ* trace element data from minerals were not available, however. Whereas major element trends were successfully modelled, trace element concentrations of the daughter compositions were inconsistent with those found in nature. The calculated residual liquids for the most mafic compositions (models A–D) showed discrepancies of tens of per cent for several trace elements, regardless of whether an element was compatible or incompatible. For instance, the Sr concentration of model A had a 27% deviation from the targeted daughter composition. In those cases where Sr appeared to be consistent with the model, other elements showed strong discrepancies. Ablay *et al.* (1998) therefore invoked selective addition of zeolite and hydrothermally altered facies, although these end-members and the contamination mechanism were not specified any further. In such a scenario, however, the oxygen isotope ratios of mafic lavas ought to display $\delta^{18}O$ values significantly displaced from normal magmatic ratios (Donoghue *et al.* 2008), which cannot be confirmed (Wiesmaier *et al.* 2012).

Also with respect to the most mafic lavas of the sequence, for which contamination by a shallow component has been ruled out (Wiesmaier *et al.* 2012), the trace element models of Ablay *et al.* (1998) failed to reproduce natural compositions. Nevertheless, low Mg-numbers and disequilibrium with mantle olivine for even the most mafic products of the Teide–Pico Viejo complex (e.g. Ablay *et al.* 1998) require some magmatic differentiation.

Thermobarometric studies

Current knowledge of Teide's plumbing system places constraints on conditions for differentiation of mafic magmas. Magma ascent at Teide is controlled by a rift zone system that probably lacks interposed magma chambers (Carracedo 1994, 1996), and is thus considered rapid. Thermobarometric studies suggested that mafic magmas of the Canaries differentiated at upper mantle and lower crustal levels (Ablay *et al.* 1998; Hansteen *et al.* 1998; Klügel *et al.* 2000, 2005; Galipp *et al.* 2006; Longpré *et al.* 2008; Stroncik *et al.* 2009). The recent submarine rift zone eruption on the western island of El Hierro is a case in point. Consistent with thermobarometry, magma movement was seismically traced at sub-Moho depths for almost three months. A few days before the onset of the eruption, the seismic activity migrated towards the surface, indicating a fast ascent of magma through the oceanic crust and the island edifice (López *et al*. 2012). As a result, shallow, felsic contaminants can be excluded for these magmas, consistent with their monotonous Sr isotope ratios and Nd and Pb isotope ratios that are in line with mantle source variations (Wiesmaier *et al.* 2012). Because of the similar storage conditions for mafic magmas detected in different islands of the Canaries, Teide mafic lavas must have undergone very similar *P–T* histories.

Geochemistry of the Teide–Pico Viejo succession

In a partner study to the stratigraphic revision of the Teide–Pico Viejo succession by Carracedo *et al.* (2007), the entire succession has been analysed for major and trace elements (Rodríguez-Badiola *et al.* 2006). Both stratigraphy and geochemical data are a critical addition to the previously published closed-system model by recognizing more eruptions as part of the Teide–Pico Viejo succession than Ablay *et al.* (1998). The mafic lavas of the Teide–Pico Viejo succession (here regarded as having <53 wt% SiO_2) are separated into two groups, one with low Sr and low Zr concentration (<350 and <1000 ppm, respectively) and the other with high Sr and high Zr concentration (>300 and >1000 ppm, respectively; Fig. 2). The two groups, low Sr–Zr and high Sr–Zr, cannot be distinguished systematically by incompatible trace element ratios or other geochemical parameters, although the high Sr–Zr lavas tend to be the more evolved. The inconsistencies in trace element concentrations that the Ablay *et al.* (1998) fractionation models showed for the Teide–Pico Viejo succession are thus exemplified by Sr and Zr.

Plagioclase possesses high melt–mineral partition coefficients for Sr (Blundy & Wood 1991) and is thus especially suitable as a tracer of differentiation from low Sr–Zr to high Sr–Zr mafic lavas that are present at Teide. Strontium is incompatible in olivine and considerably less compatible in the phases of interest (amphibole and clinopyroxene) than it is in plagioclase. It is therefore possible to monitor magmatic processes that occur within the feldspar stability field by means of Sr concentration data from feldspar. Using Zr, in turn, provides a measure of the degree of differentiation that is independent of any of the phases that potentially fractionate in the mafic regime, as Zr is incompatible in the alkaline series up to felsic compositions (Watson & Harrison 1983; Wolff & Toney 1993). Because Sr and Zr are both enriched with degree of differentiation in the Teide–Pico Viejo mafic lavas, an initial hypothesis may be the incompatible behaviour of Sr in absence of plagioclase.

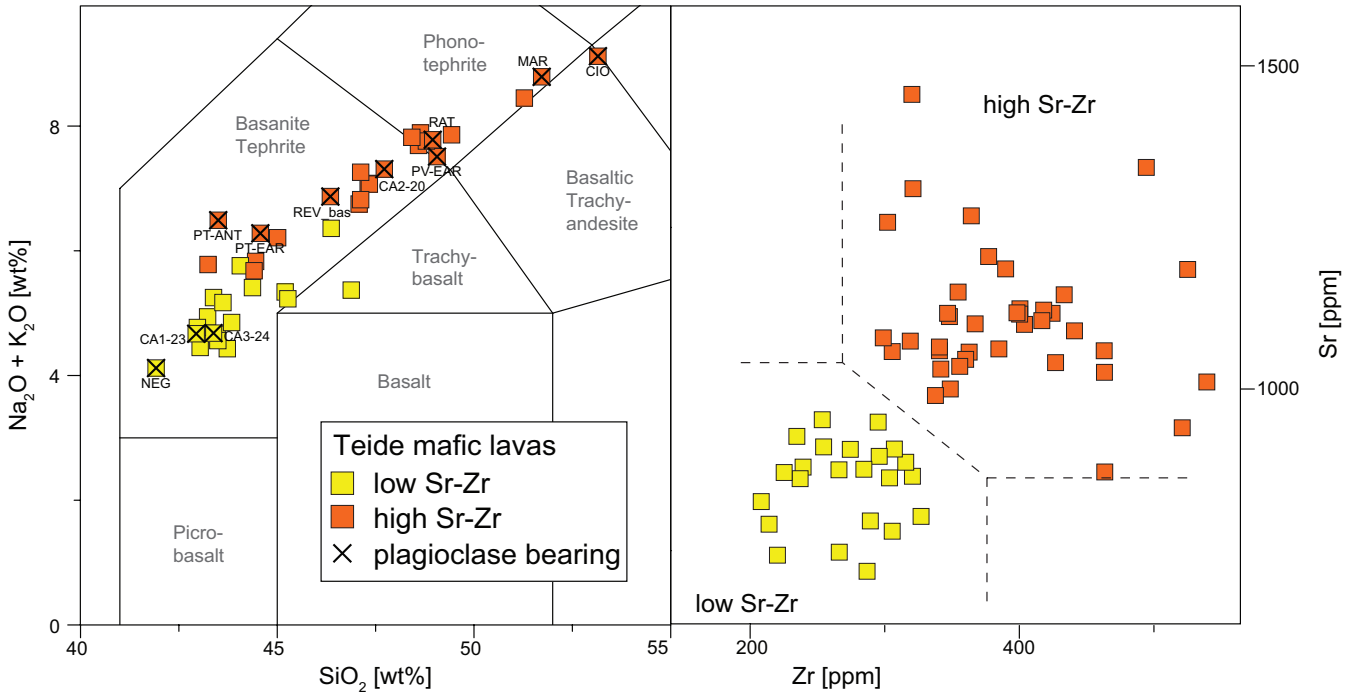

Fig. 2. (**a**) Total alkali v. silica diagram of the Teide–Pico Viejo succession after Wiesmaier *et al.* (2012). Data points marked with an '×' are samples that contain plagioclase. (**b**) Lava samples show systematic trace element behaviour with increasing degree of differentiation: both Sr and Zr are progressively enriched with increasing degree of differentiation. Mafic Teide lavas are hence placed into low Sr–Zr and high Sr–Zr sub-groupings.

This explanation is offset, however, by the presence of plagioclase in some of the lavas of both groups, so that Sr enrichment and absence of plagioclase do not correlate (see Fig. 2).

Methods

Feldspar microanalysis

Feldspars of the Teide–Pico Viejo succession have been analysed for major and trace element concentrations in single zones of each crystal. Major element analyses were performed with a Cameca SX-50 and trace element analyses using a New Wave™ UP-213 Nd:YAG laser ablation unit that was coupled to a ThermoFinnigan Element2™ inductively coupled plasma mass spectrometer. Both types of measurements were carried out at the GeoAnalytical Laboratory of Washington State University, USA. Details of the method have been provided by Olin & Wolff (2010) and Wiesmaier (2010). Compositions representative of the feldspar crystals found in Teide mafic lavas are given in Table 1.

Closed-system modelling

A revised fractional crystallization model for Teide mafic lavas is presented. The input parameters and the conceptual approach represent the framework of the model and are thus outlined in more detail. The 'multiple-step' strategy of Ablay *et al.* (1998) was adopted, using a least-squares regression analysis and a mass-balance calculation for every modelled step. Rayleigh fractionation has been assumed. Regarding the narrow range of SiO_2 concentrations (<53 wt%), two steps were calculated, similar to the Ablay *et al.* (1998) approach. The first model step is calculated to simulate evolution from the most mafic, low Sr–Zr lava towards the high Sr–Zr group. The second step models the variation across the high Sr–Zr group (Fig. 3).

Whole-rock Fe_2O_3 data have been recalculated to Fe_2O_3 and FeO using an Fe^{2+}/Fe^{3+} ratio of 2.16, which was measured for Teide basanite (Ridley 1970). Whole-rock oxides were normalized to 100% on a water-free basis. All other major element mineral data are from Ablay (1997), and the minor oxides SrO and BaO from that source have been recalculated to ppm. Clinopyroxene mineral data have been complemented by average Sr and Zr trace element concentrations in clinopyroxene from a Las Cañadas basanite (sample TF58 with 44 wt% silica; Neumann *et al.* 1999). Of the 10 phenocryst phases identified in the entire Teide–Pico Viejo succession, six are present in the mafic lavas: olivine (ol), clinopyroxene (cpx), plagioclase (plag), apatite (ap), titano-magnetite (mt) and ilmenite (ilm) (Ablay *et al.* 1998). This fractionation assemblage is varied according to the least-squares regression calculation and with plagioclase being included or not depending on the phase assemblage of the respective parent composition.

Average feldspar compositions of low and high Sr–Zr lavas are from Wiesmaier (2010) and the major element data for the remaining minerals have been given by Ablay (1997). A representative set of feldspar data is shown in Table 1. In summary, mineral compositions in the low Sr–Zr group are $Fo_{79–84}$ (ol), $Wo_{38–43}En_{46–51}Fs_{8–11}$ (cpx), $An_{73–84}$ (plag), $Usp_{43–70}$ (mt) and $Ilm_{87–94}$ (ilm). Apatites occur as inclusions in cpx and are mostly hydroxy-fluorapatites. Mineral compositions in the low Sr–Zr group are of low variability and have thus been averaged to achieve a bulk extract. Mineral compositions in the high Sr–Zr group are $Fo_{52–83}$ (ol), $Wo_{39–47}En_{41–52}Fs_{5–14}$ (cpx), $An_{5–62}$ (plag), $Usp_{43–70}$ (mt), $Ilm_{87–94}$ (ilm) and, similar to the low Sr–Zr group, apatites occur as inclusions in cpx and are hydroxy-fluorapatites. The composition of this bulk extract varies across the 16 calculated models depending on the respective least-squares regression coefficients.

Table 1. *Representative selection of analyses of feldspar from low and high Sr–Zr lavas of Teide–Pico Viejo*

	Low Sr–Zr lavas				High Sr–Zr lavas		
Sample:	CA1-75-1-01-r	CA1-75-1-12-c	CA3-22-1-01-r	NEG-50-2-01-r	REV-71-2-01-r	CIO-77-1-01-r	CIO-77-1-16
Distance from core (μm):	1900	0	661	507	373	2120	197
EMP (wt%)							
SiO_2	46.09	50.49	45.39	48.51	58.49	60.75	55.34
Al_2O_3	33.34	30.50	34.35	32.34	25.57	23.41	26.58
Fe_2O_3	0.68	0.69	0.80	0.86	0.46	0.57	0.46
K_2O	0.29	0.43	0.20	0.19	0.85	1.04	0.53
Na_2O	1.95	3.78	1.61	2.78	7.18	7.76	5.97
CaO	15.73	12.10	16.78	15.14	6.64	5.06	8.71
BaO	0.01	0.00	0.00	0.00	0.14	0.37	0.02
Total	98.10	98.00	99.13	99.83	99.34	98.96	97.62
An (mol%)	80.23	62.17	84.19	74.22	32.16	24.88	43.23
Ab	18.00	35.18	14.59	24.70	62.91	69.03	53.63
Or	1.78	2.65	1.22	1.08	4.92	6.10	3.14
LA-ICP-MS (ppm)							
Rb				0	2	1	2
Ba	169	136	102	209	1232	850	1020
La	6	5	3	4	17	13	10
Ce	10	8	5	5	20	18	13
Pr	1	1	–	1	1	1	1
Nd	3	2	2	2	3	3	2
Eu	1	1	–	–	2	1	1
Y	–	–	–	–	–	–	–
Pb	–	1	–	–	3	3	3
Sr	2703	2642	1944	2106	2378	3350	3050
Ti	481	461	510	855	634	680	500
Mg	551	584	630	879	155	241	247

The complete dataset of the Teide–Pico Viejo succession comprises 785 electron microprobe (EMP) and 766 laser ablation inductively coupled plasma mass spectrometry (LA-ICP-MS) data points; details on the method have been given by Wiesmaier (2010). Hyphens in trace element data denote values below 0.4 ppm that have been rounded down to zero.

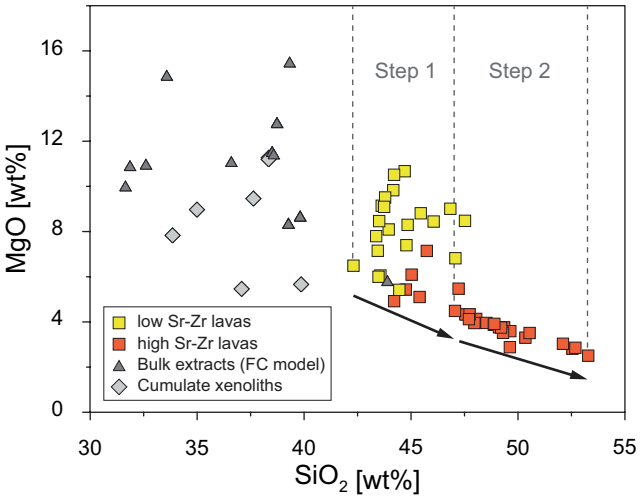

Fig. 3. SiO_2 v. MgO of the low and high Sr–Zr lava samples, the bulk extract compositions from the calculcated closed-system model, and Tenerife cumulate xenolith compositions from Neumann *et al.* (1999). Step 1 describes the evolution from the most primitive low Sr–Zr composition to the high Sr–Zr lavas and step 2 designates the variation within the high Sr–Zr lava compositions.

Strontium is compatible in plagioclase, making plagioclase the key mineral for mass-balance models that include Sr concentrations. The new high-precision feldspar data provided by Wiesmaier (2010) thus guarantee a more realistic estimation of the Sr contents of the fractionated assemblage. Throughout the two-step model, the presence of plagioclase was systematically varied and four permutations were calculated: (parent + plag)/(daughter + plag), (parent + plag)/(daughter − plag), (parent − plag)/(daughter + plag), (parent − plag)/(daughter − plag). For each of these permutations, four eligible parent/daughter pairs were selected, accounting for a total of 16 calculated fractionation models. This strategy allowed evaluation of the compositional effects that fractional crystallization may exert on the natural parent compositions at a high resolution.

Determination of melt compositions and crystallization temperatures

Empirical relationships have been employed to constrain the crystallization temperature of plagioclase, which is an essential input parameter for the subsequently presented EC-RAFC model. Several studies have quantified elemental plagioclase–melt partitioning based on synthetic and natural examples (Blundy & Wood 1991; Bindeman *et al.* 1998; Bédard 2006). Namur *et al.* (2012) revised the empirical relations for plagioclase–melt equilibria, using a database of results from 1 atm anhydrous experiments. However, their regression models are tied to more than one compositional parameter, for which reason they do no lend themselves to a reverse modelling approach, despite the accuracy of their model being superior in forward modelling.

Table 2. *Parameters used for melt modelling equations*

Y	*X*	*a*	±*a*	*b*	±*b*	Comment	Reference	Reference equation number
Melt MgO (wt%)								
ln(MgO)	X_{An}	0.04448	±0.00158	0.42132	±0.07065	For dry melts, MgO >1 wt%	Bédard 2006	3a
ln(MgO)	X_{An}	0.50206	±0.09061	0.10090	±0.10362	For dry melts, MgO >1 wt%	Bédard 2006	3b
ln(MgO)	X_{An}	0.10639	±0.00444	0.57229	±0.13285	Wet melts	Bédard 2006	3c
Crystallization temperature (°C)								
10000/*T*	ln(MgO)	−0.95668	±0.01728	10.3758	±0.0232		Bédard 2006	5a
1/*T*	ln(MgO)	-2.04×10^{-4}		7.92×10^{-4}			Bindeman *et al.* 1998	3

All calculations follow the equation $Y = aX + b$.

In turn, the empirical relationships of Bindeman *et al.* (1998) and Bédard (2006) allow a reconstruction of key parameters for subsequent modelling of magmatic differentiation. Based on pre-existing natural and experimental data, Bédard (2006) developed several empirical equations that relate the anorthite content of plagioclase to the MgO concentrations of the melt from which the analysed plagioclase compositions crystallized:

$$\ln(\mathrm{MgO}) = \frac{X_{An} - (b \pm \Delta b)}{a \pm \Delta a} \quad (1)$$

where *a* is the slope of the calculated regression and *b* is the intercept of the regression on the *y*-axis. The bivariant nature of the equations permits reverse modelling of various chemical and physical parameters of the parent melt of the analysed Teide–Pico Viejo plagioclase crystals. In a second step, the temperature at which a given zone of feldspar crystallized may be calculated from the previously calculated MgO composition of the melt:

$$\frac{10000}{T} = a\ln(\mathrm{MgO}) + b. \quad (2)$$

All parameters used for each modelling step are listed in Table 2.

EC-RAFC starting point: justification of input parameters

An EC-RAFC model is presented, which requires a wide variety of input parameters such as crystallization or fusion enthalpies, magma and contaminant temperature and composition. These parameters are justified in the methods section to separate them from results and subsequent interpretation. The theoretical background to the EC-RAFC model has been laid out by Spera & Bohrson (2001, 2002, 2004) and models of natural systems were presented by Bohrson & Spera (2001, 2003) and (Fowler *et al.* 2004). All input parameters for the EC-RAFC model are summarized in Table 3.

Envisaged scenario. In the EC-RAFC model presented here, a batch of mafic magma is in thermal and compositional equilibrium with the cumulate rock that precipitated from the magma earlier on. Recharge with a new batch of superliquidus, low Sr–Zr magma (hereafter referred to as 'recharge magma') induces thermal and compositional disequilibrium and subsequent equilibration. The hotter recharge magma thus induces anatexis in the cumulate. Subsequently, the reservoir cools again, and fractionation resumes production of cumulate. It is tested whether or not this scenario is able to reproduce the composition of a high Sr–Zr magma.

Temperature constraints. Owing to the constant heat flow from mantle to crust, the temperature fluctuations at Moho depth will be small and the cumulate rock is probably kept at near-solidus temperatures, reducing the ΔT necessary to initiate anatexis. Hydrothermal cells would not be expected at Moho depth, for which reason an isenthalpic AFC scenario is assumed (see Reiners *et al.* 1995). As a consequence, we assume a narrow temperature interval of $\Delta T = 23$ K for the EC-RAFC scenario between the temperature of the hot recharge magma and thermal equilibration.

A temperature of 1300 °C was assigned to the liquidus and as the initial temperature of the recharge magma. Pristine magma temperature was assumed to be 1290 °C ($T_l^m = T_m^0$), consistent with thermobarometric constraints (Ablay *et al.* 1998) and the results from anorthite temperature modelling presented here. The difference of −10 K to the recharge magma provides an increase in thermal energy upon recharge. The equilibration temperature has been set to 1277 °C; that is, below the initial temperature of pristine magma to trigger crystallization and above the cumulate's solidus to allow anatexis in the cumulate. The solidus temperature T_s has been set to 1250 °C to yield small degrees of partial melt from the gabbroic cumulate (Table 3). Long-term magma chamber replenishment should balance with intermittent expulsion of magma. Hence, the thermal parameters were set to even out the mass of anatectic melt and cumulate that is produced (so as not to clog the magma chamber or remelt all the cumulate).

Composition of magma and cumulate. The Sr, Nd, Zr and Ni concentrations of the initial and the recharge magma have been calculated as the average of composition of the low Sr–Zr lavas (data from Rodríguez-Badiola *et al.* 2006). As contaminant, we assume gabbroic and kaersutite-bearing cumulate rock, which has been found as xenoliths in Tenerife mafic magmas (Neumann *et al.* 2000). These cumulates have been interpreted to form by fractional crystallization of mafic alkaline magma at depth and thus represent a potential end-member for assimilation during recharge. The average composition of these analysed cumulate samples has been used as contaminant data in the model (Table 3).

Partition coefficients. The trace elements Sr and Zr were modelled together with Nd and Ni, the latter two as a control for REE behaviour and compatible elements. To ensure comparability between the EC-RAFC and the closed-system model, the same

Table 3. *Parameters for EC-RAFC modelling*

Thermal parameters			
Pristine magma liquidus temperature, $T_{l,m}$	1290 °C	Crystallization enthalpy, Δh_m (J kg^{-1})	398300
Pristine magma initial temperature, T_m°	1290 °C	Isobaric specific heat of magma, $C_{p,m}$ (J kg^{-1} K^{-1})	1479
Recharge magma liquidus temperature, $T_{l,m}$	1300 °C	Crystallization enthalpy, Δh_r (J kg^{-1})	398300
Recharge magma initial temperature, T_m°	1300 °C	Isobaric specific heat of magma, $C_{p,m}$ (J kg^{-1} K^{-1})	1479
Assimilant liquidus temperature, $T_{l,a}$	1300 °C	Fusion enthalpy, Δh_a (J kg^{-1})	364000
Assimilant initial temperature, T_a°	1210 °C	Isobaric specific heat of assimilant, $C_{p,a}$ (J kg^{-1} K^{-1})	1307
Solidus temperature, T_s	1250 °C		
Equilibration temperature, T_{eq}	1277 °C		
Recharge M_r°	0.5		

	Sr	Nd	Zr	Ni
Compositional parameters				
Pristine magma initial concentration (ppm), C_m°	861	48	237	150
Pristine magma trace element distribution coefficient, D_m	0.89	0.65	0.18	12.6
Recharge magma initial concentration (ppm), C°	861	48	288	147
Recharge magma trace element distribution coefficient, D_r	0.89	0.65	0.18	12.6
Assimilant initial concentration (ppm), C°	1754	87	154	150
Assimilant trace element distribution coefficient, D_a	0.89	0.65	0.18	12.6
Average concentration of high-Sr/high-Zr magma (ppm)	1086	69	389	38

Melt functions were non-linear, and non-linear logistical parameters were $a = 450$, $b = -11$ for pristine and recharge magma, and $a = 400$, $b = -11$ for the contaminant.

bulk partition coefficients as calculated in the closed-system model were employed. These were computed using the trace element data from plagioclase, partition coefficients from the literature for Nd and Ni concentrations in olivine, magnetite, ilmenite and apatite (Fujimaki 1986; Nielsen 1992; Ewart & Griffin 1994; Zack & Brumm 1998; Adam & Green 2006), and analysed olivine and clinopyroxene compositions from Tenerife basanites (Neumann *et al.* 1999). Bulk partition coefficients calculated from the closed-system models yielded the following ranges: Sr 0.13–0.89 (average 0.5) and Zr 0.18–0.60 (average 0.41). Furthermore, bulk partition coefficients for Nd and Ni were calculated to serve as input parameters for the EC-RAFC model; Nd yielded 0.5–3.10 (average 1.20), and Ni 4.0–12.6 (average 8.0). The bulk partition coefficients employed in the EC-RAFC model are consistent with the ranges of bulk D values shown here (Table 3).

Thermodynamic parameters. All end-member compositions and their fusion and crystallization enthalpies are constrained by natural data. Specific heat capacities and crystallization or fusion enthalpies were calculated from the oxide and mineral values given by Spera & Bohrson (2001), using the average compositions of the low Sr–Zr compositional group combined with normative abundances for Tenerife basanite given by Araña *et al.* (1994).

The cumulate enthalpies were constrained from the petrographic information provided by Neumann *et al.* (2000). We assumed mineral percentages of 30% plagioclase, 30% kaersutite, 20% clinopyroxene and 15% oxides plus 5% minor phases as a typical example of a Tenerife gabbroic cumulate. Combining these modal abundances with the mineral data given by Neumann *et al.* (2000) reproduced the average of gabbro cumulate analyses within 2 wt% for each of the oxides and was considered a reasonable approximation. These modal abundances were then used to calculate the bulk specific heat capacity and the crystallization or fusion enthalpy of this model contaminant.

Inherent EC-RAFC parameters. In mantle and cumulate xenoliths, interstitial melt is frequently found, which implies that melt extraction is usually incomplete. The normalized fraction of anatectic melt extracted from the contaminant (χ) was thus assumed to be 0.95. The relative mass of recharge M_r^0 is kept at 0.5 to simulate a batch of recharge magma smaller than the total volume of the magma reservoir. Partition coefficients were kept constant throughout the model, as a relatively small compositional window of differentiation is simulated ($\Delta SiO_2 = 3$ wt%).

Results

The recalculated closed-system model

Modelling step 1: low Sr–Zr to high Sr–Zr compositions. Three combinations of parent–daughter lava compositions have been calculated for each of the four scenarios, giving 12 models in total for step 1. Bulk extracts resembled the compositions of gabbroic xenoliths from Tenerife (see Neumann *et al.* 1999; Fig. 3). Examples of F values, bulk extract compositions and bulk partition coefficients of scenario 1 are shown in Table 4.

Scenario 1: both parent and daughter bear feldspar. An overall good fit for major elements was achieved. Exceptions were TiO_2 and MnO, which were underestimated by −14 to −16% and −17 to −19%, respectively. Trace elements Zr and Sr were underestimated by −2 to −4% and −5 to −17%, respectively.

Scenario 2: both parent and daughter are feldspar-free. Of the major elements, TiO_2 was underestimated by −12 to −15% and CaO by −6 to −9%. K_2O varied by +3 to −11%. Al_2O_3 and FeO were overestimated by +6 to +9% and MgO varied from −11% to +14%. Strontium deviated variably by zero to −18% and Zr was underestimated by −15 to −20%.

Scenario 3: parent bears feldspar and daughter is feldspar-free. Silica was overestimated by +1%, translating to *c*. +0.5 wt% difference. Al_2O_3 was underestimated by zero to −11%, whereas Fe_2O_3 and FeO were overestimated by +6 to +16% and +4 to +12%, respectively. Strontium was underestimated by −18 to −22% and Zr by −1 to −6%.

Scenario 4: parent is feldspar-free and daughter bears feldspar. This is the scenario with the overall highest variability in major elements. TiO_2, MnO, Na_2O, K_2O and P_2O_5 were underestimated by more than −15%, whereas Al_2O_3, Fe_2O_3 and FeO either fitted well or were overestimated by more than +10%. Strontium was underestimated by

Table 4. F *values, bulk extract compositions and bulk partition coefficients of selected trace elements for scenario 1 of the closed-system model*

Modelling step:	Low Sr–Zr to high Sr–Zr (mafic)			High Sr–Zr (mafic) to high Sr–Zr (evolved)
Model:	A	B	C	D
Parent:	Montaña Cascajo, phase 1 TFC-249	Montaña Cascajo, phase 3 TFC-287	Montañas Negras TFC-276	Montaña Reventada basanite TFC-243
Daughter:	Montaña Reventada basanite TFC-243	Montaña Reventada basanite TFC-243	Montaña Reventada basanite TFC-243	Montaña de Chío TFC-540
Bulk *F* (%)	39.73	37.78	48.82	33.68
ol (low Sr–Zr)	5.29	3.87	1.71	
cpx (low Sr–Zr)	19.11	18.11	23.74	
plag (low Sr–Zr)	8.00	8.36	14.10	
ol (high Sr–Zr)				2.05
cpx (high Sr–Zr)				14.15
plag (high Sr–Zr)				10.12
mt	7.29	7.44	9.27	4.96
il	0.00	0.00	0.00	0.84
ap	0.04	0.01	0.00	1.55
Bulk extract composition (wt%)				
SiO_2	38.73	38.50	39.81	39.27
TiO_2	5.18	5.45	5.33	5.54
Al_2O_3	9.73	10.34	12.28	11.01
Fe_2O_3	6.46	6.83	6.72	5.66
FeO	12.45	12.51	11.13	10.87
MnO	0.24	0.25	0.23	0.26
MgO	12.82	11.54	8.68	8.36
CaO	12.87	12.98	13.80	14.61
Na_2O	1.23	1.32	1.66	2.01
K_2O	0.24	0.27	0.35	0.45
P_2O_5	0.04	0.01	0.00	1.96
ppm				
Sr	484.16	520.32	655.60	705.24
Zr	78.99	78.72	79.84	152.56
Nd	25.66	24.37	24.31	96.81
Ni	700.99	653.35	476.63	456.86
Bulk D_{Sr}	0.56	0.59	0.83	0.63
Bulk D_{Zr}	0.33	0.33	0.37	0.44
Bulk D_{Nd}	0.53	0.50	0.58	1.41
Bulk D_{Ni}	6.33	7.62	6.57	103.36

Scenario 1 is for a feldspar-bearing parent and a feldspar-bearing daughter composition. Models A, B and C are for step 1 (i.e. a low Sr–Zr parent and a high Sr–Zr daughter). Model D is for step 2, differentiation within the high Sr–Zr group.

−1 to −22% and Zr by −21 to −27%, so that a suitable combination of solutions for both elements was never achieved.

Modelling step 2: differentiation within the high Sr–Zr group. One parent–daughter combination has been calculated for each of the four scenarios, which makes four models in total for step 2. An example of data for scenario 1 is given in Table 3.

Scenario 1: both parent and daughter bear feldspar. Stringently applying the criterion of lowest average least squares caused SiO_2 to be underestimated by −4%. TiO_2, MgO, Fe_2O_3 and FeO were within ±1% of the natural daughter composition, whereas the remaining oxides showed deviations between 4 and 36%. Strontium was overestimated by +30% and Zr underestimated by −17%.

Scenario 2: both parent and daughter are feldspar-free. SiO_2, MgO, CaO and Na_2O were well reproduced, whereas the remaining oxides showed deviations between 6 and 76%. Strontium was overestimated by +40% and Zr underestimated by −30%.

Scenario 3: parent bears feldspar and daughter is feldspar-free. SiO_2, TiO_2, Al_2O_3, Fe_2O_3, FeO, MnO and P_2O_5 were well reproduced, whereas MgO, CaO, K_2O and Na_2O showed deviations between 6 and 23%. Strontium and Zr were both overestimated, by +17% and +34%, respectively.

Scenario 4: parent is feldspar-free and daughter bears feldspar. SiO_2 was underestimated by −3%. TiO_2, Fe_2O_3, FeO, MgO and CaO were well reproduced, whereas Al_2O_3, MnO, CaO, K_2O, Na_2O and P_2O_5 showed deviations between 6 and 23%. Strontium was overestimated by +34% and Zr underestimated by −36%.

Throughout the differentiation of mafic magma, Sr appears to be incompatible in bulk owing to the predominant fractionation of non-Sr incorporating minerals (ol, cpx, mt). An enrichment of Sr along with Zr can thus be achieved in principle, but in 14 out of 16 models Sr is not enriched to the degree necessary to reproduce natural daughter compositions. This incompatible behaviour is reflected in the bulk partition coefficients that were calculated for Sr and Zr (Table

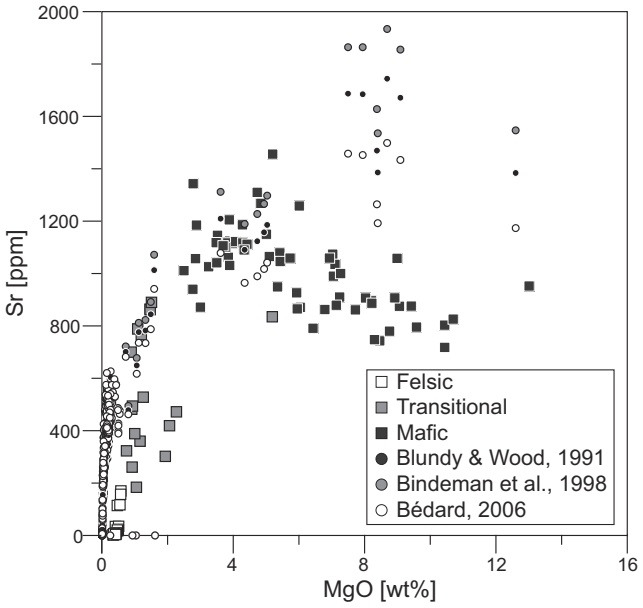

Fig. 4. Modelled melt compositions in comparison with existing whole-rock data from Rodríguez-Badiola *et al.* (2006). The melt MgO concentrations were calculated using the equations of Bédard (2006). Squares are natural data and circles are modelled data. Between MgO of 1 and 6 wt%, modelling melt Sr compositions with the equation parameters of Blundy & Wood (1991) replicates the natural data (black circles).

3). When Sr is enriched sufficiently in two out of 16 models, either Zr remains too depleted or TiO_2 is not reproduced by the model.

Calculation of crystallization temperature and melt Sr concentration

The modelling of melt compositions yielded useful information for the subsequently calculated EC-RAFC model. Using the equations from Blundy & Wood (1991) and Bédard (2006), a temperature interval of 645 °C (−45, +50) to 1257 °C (−170, +255) for the Teide–Pico Viejo suite was computed. For the calculation of melt MgO, the equations for both wet and dry melts of Bédard (2006) were tested. The results for dry melt MgO are inconsistent with natural Teide–Pico Viejo data (Bédard's equation (3b); Table 2), but the equation for wet melts reproduces the natural MgO data very well, particularly between 1 and 6 wt% MgO (Fig. 4). Below 1 wt% MgO, the calculation slightly underestimates the MgO concentration of the most evolved lavas; this is probably an artefact as these values are computed using the anorthite content of anorthoclase crystals.

EC-RAFC model

Using the parameters summarized in Table 3, the following results were derived. The mass fraction of anatectic melt M_a* generated from the contaminant is 0.39, whereas the mass fraction of produced cumulate M_c is 0.338. The mass fraction of solidified recharge magma M_{en} amounted to 0.127. This equals a total mass fraction of produced solids of 0.465 versus 0.39 for anatectic melt. The amounts of cumulate and anatectic melt formed in one model step are a result of the elevated solidus temperature, where relatively small changes in temperature (*c.* 10 °C) trigger significant amounts of crystallization.

Modelled trace element concentrations reproduced the concentrations of high Sr–Zr lavas, with Sr increasing to 1132 ppm, Zr to 326 ppm, Nd to 68 ppm and Ni decreasing to 7 ppm. Graphs for T_{magma} v. M_a*, M_a*/M_c, Zr and Sr, respectively, are shown in Figure 5. Uncertainties in trace element calculations were calculated in the code and did not exceed 4%, except Ni, which below a concentration of 37 ppm showed progressively larger errors of up to 12%.

Discussion

New closed-system models

The closed-system model fits best when combining a plagioclase-bearing parent with a plagioclase-bearing daughter. This scenario is shown in Fig. 6. Both Sr and Zr concentrations are slightly underestimated by this model compared with the natural daughter composition, but are reasonably close fits to the high Sr–Zr lava data. In detail, however, TiO_2 is systematically underestimated in all models of the (parent + plagioclase)/(daughter + plagioclase) combination. Furthermore, this particular model accounts for only a scenario in which plagioclase is present in the parent as well as in the daughter phase assemblages. All other permutations of the system (parent ± plagioclase)/(daughter ± plagioclase) show trace element concentrations that systematically underestimate either Sr or Zr concentrations, or both, or fail to reproduce several oxides. The closed-system models thus appear to require the presence of plagioclase in both parent and daughter, a condition only rarely fulfilled in the Teide–Pico Viejo succession, as only few of the mafic lavas have plagioclase.

Together with the older model of Ablay *et al.* (1998), which showed considerable inconsistencies in the reproduction of trace element concentrations because of lack of mineral trace element data, the updated closed-system model shows that the closed-system approach may be too simplified to reproduce the complex mechanism of magmatic differentiation. Although the closed-system models for mafic Teide lavas appear to provide a reasonable approximation for their major element variations, we note that calculating a good fit for least-squares regression models usually presents no difficulty. This is especially true when the major element concentrations of the phase assemblage in the samples have been measured. Experience shows that good fits are achieved even when 'foreign' mineral data from other settings of comparable tectonic origin are used, probably as a result of the stoichiometric nature of mineral major element data. Mass-balance models based purely on major elements do not provide good constraints on details of differentiation processes. Likewise the incorporation of high-precision plagioclase trace element data into the model of Teide mafic lavas fails to provide 100% accurate fits. A common argument advanced to explain these inaccuracies is variation in the compositions of the fractionated mineral solid solutions. However, given the narrow compositional window that the model covers, it appears unlikely that mineral variations alone can be held responsible for model inaccuracies, as the average mineral compositions extracted from the parent composition were chosen to reflect the data from the natural samples. Considering the plethora of least-squares regression models attempted here, it is concluded that major and trace element closed-system fractionation models are insufficient to explain all major and trace element variations found in mafic Teide lavas (SiO_2 <53 wt%).

Reverse modelling of plagioclase crystallization temperature

The empirical models of Bédard, Blundy and Bindeman described above permit the calculation of temperature and melt Sr concentrations at the time of plagioclase crystallization. Bindeman *et al.* (1998) constrained their set of equations to an anorthite content between 40 and 80 mol%, because in this range most natural data show a linear relationship between An content, crystallization temperature and

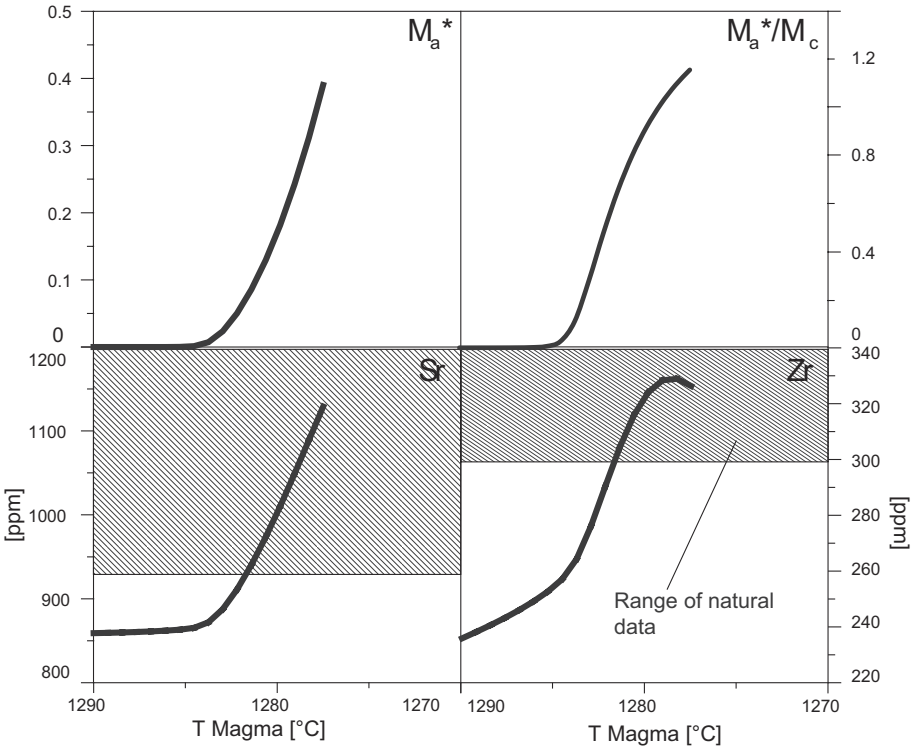

Fig. 5. The evolution of melt compositions from EC-RAFC modelling. M_a* (mass of anatectic melt generated) and M_c (mass of cumulate formed) are dimensionless. The *x*-axis is magma temperature; the system thermally equilibrates itself from higher to lower temperatures (left to right). All parameters comply with the natural compositions of the high Sr–Zr lavas.

melt Sr concentrations. Modelled crystallization temperatures yield <1257 °C (−170, +255) for low Sr–Zr lavas, whereas high Sr–Zr lavas appear to have crystallized their feldspars below 1009 °C (−109, +146) (Fig. 7). Ablay *et al.* (1998) conducted olivine thermometry, which yielded 1230 °C and 1210 °C for two alkali basalts (±40 °C; equivalent to the low Sr–Zr group), and 1180 °C for an evolved basanite (±40 °C; equivalent to the high Sr–Zr group). Their clinopyroxene–liquid estimates on the same samples yielded 1224 °C, 1211 °C and 1197 °C, respectively (all ±27 °C).

The high-*T* lavas contain only few and small plagioclases (Montaña Cascajo CA3 and CA1, Montañas Negras NEG) and most probably record the onset of plagioclase crystallization in the Teide–Pico Viejo system. The temperatures modelled by correlation with An content in plagioclase are thus consistent with independent measurements from the same eruptive sequence, albeit at the penalty of much larger errors. Furthermore, the agreement of the empirical feldspar models with the thermometric estimates of Ablay *et al.* (1998) is better at more calcic feldspar compositions, whereas the crystallization temperatures calculated for plagioclase from high Sr–Zr lavas ($An_{<60}$) overlap in error by only a small margin. Therefore, feldspar thermometry is consistent with a continuous evolution from hotter, more primitive magma with low Sr and Zr concentrations to cooler, more evolved magma with high Sr and Zr concentrations. Notably, the heat loss during evolution from low to high Sr–Zr groups recorded by olivine thermometry and cpx–liquid estimates appears comparatively small.

EC-RAFC model

The EC-RAFC code was able to reproduce the enrichment of Sr and Zr by crystallization of low Sr–Zr magma and simultaneous assimilation of low-volume anatectic melts from cumulate rocks. The resulting melt possessed trace element compositions characteristic of the high Sr–Zr mafic lavas from the Teide–Pico Viejo succession. The equivalent of the closed-system scenario 1, model A (feldspar-bearing sample CA1 to feldspar-bearing sample REV_bas) is shown in Figure 8. Zirconium is underestimated by 6% for the daughter composition, but is consistent with the range of concentrations found at the mafic end of the high Sr–Zr group. The elements Sr, Nd and Ni are found to consistently reproduce the natural daughter composition, with the enrichment of Sr exceeding the daughter composition by 2%. It thus appears more likely that the combined mechanisms of assimilation and fractional crystallization are responsible for the enrichment of incompatible trace elements among the two observed groups of mafic lavas. This evolutionary link is not reproduced by closed-system fractionation models.

The Teide–Pico Viejo EC-RAFC model requires a mass fraction ratio of crystallized solids and anatectic melt close to unity. Only this approach achieved a modelled melt composition that replicated the natural high Sr–Zr lavas and implies that the magma chamber system must keep a balance between input and output. This is significant in terms of the ‘space problem’ discussed by O’Hara (1998): the presence of pre-existing solid material in magma systems experiencing mantle input cannot be ignored. By rigorously applying thermodynamic and chemical constraints, this study therefore provides a natural example of an ocean island plumbing system that recycles its own products in even the most mafic members of a differentiation series.

The two groups of lavas, low Sr–Zr and high Sr–Zr, are thus related by open-system processes. This implies that both groups of lavas represent different evolutionary stages of the same plumbing system. The high Sr–Zr lavas appear to have experienced extended AFC processes (i.e. thermal equilibration with authigenic cumulate

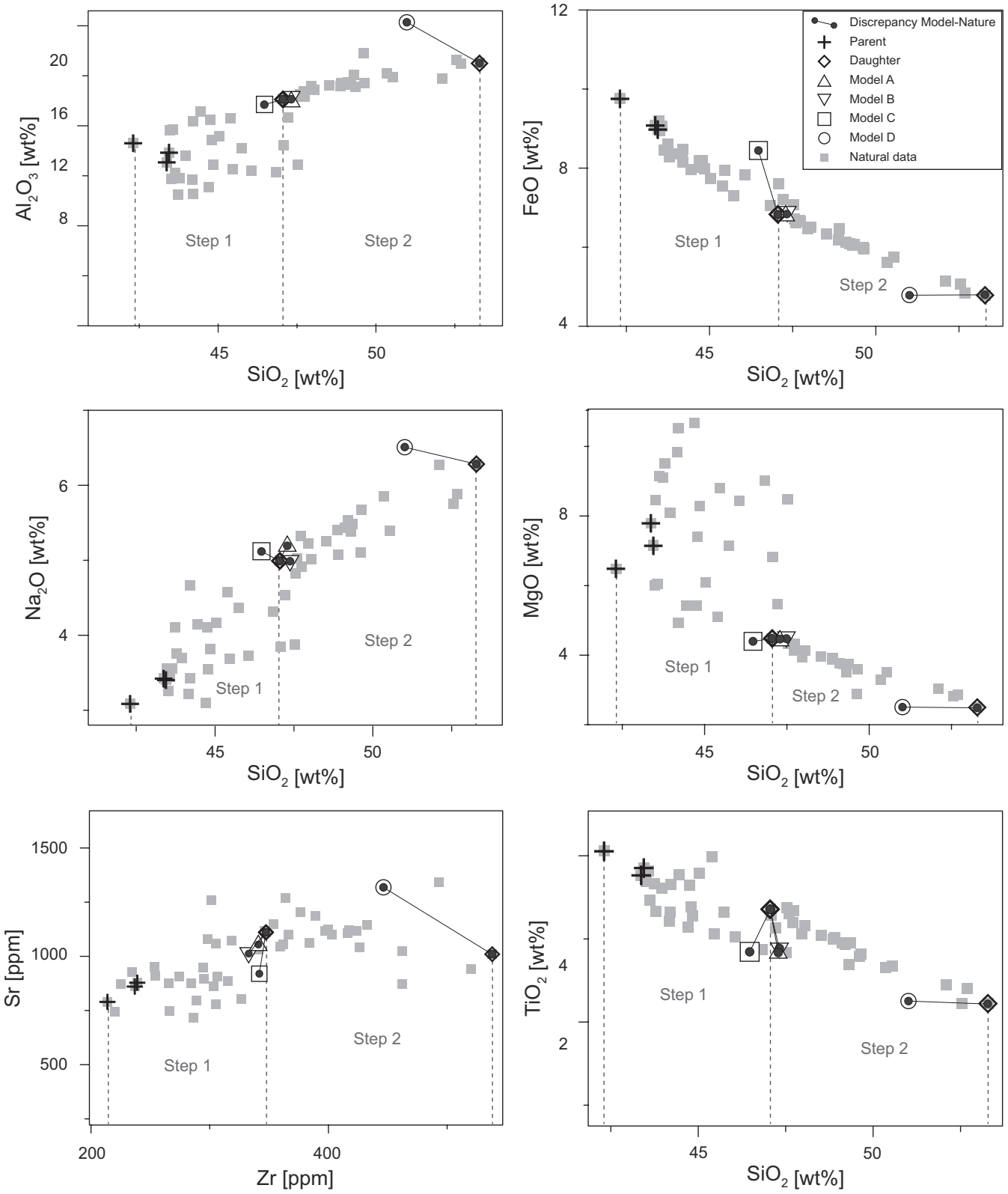

Fig. 6. Major and trace element variation plots of the Teide fractionation model presented here. Only scenario 1 is shown; that is, when both parent and daughter compositions are feldspar-bearing. Of all scenarios, scenario 1 shows the best fits to natural daughter compositions. Discrepancies between model results and natural samples are indicated by tielines. The two modelling steps (low Sr–Zr to high Sr–Zr and then differentiation within the high Sr–Zr group) are indicated in the graphs. Models A–C belong to the first step and model D to the second step.

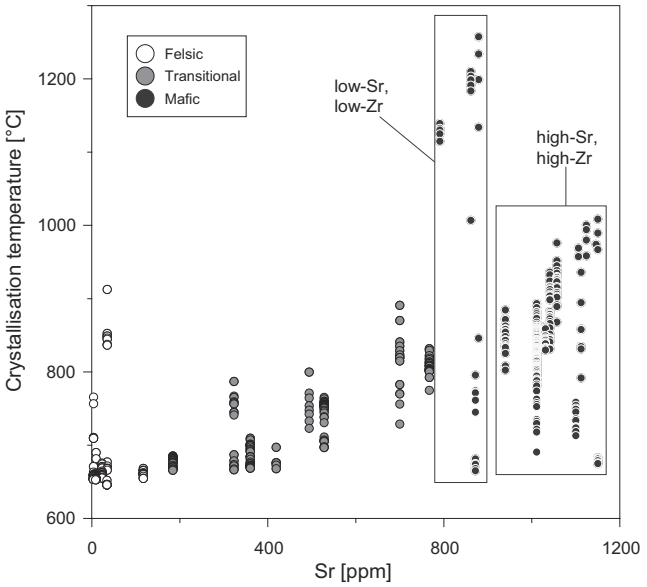

Fig. 7. Whole-rock Sr data v. modelled crystallization temperature of feldspars in the Tenerife post-collapse lavas. Mafic lavas show a pronounced high at the lower end of the Sr concentration range.

rock) and thus achieved a more evolved compositional signature, including trace element concentrations that exceed the possibilities produced by closed-system fractionation. The more primitive low Sr–Zr lavas, in turn, were less affected by AFC processes, perhaps owing to shorter residence times in lower crustal magma chambers. However, olivine from these lavas is in disequilibrium with the mantle (Ablay *et al.* 1998). Although the low Sr–Zr group seem to have experienced comparatively little modification within magma chambers, the lack of knowledge on the composition of primitive mantle melts prevents an estimation of the full degree of differentiation in these lavas. It is thus possible that the most primitive lavas of the Teide–Pico Viejo system may also have been subject to open-system equilibration with solid material.

The effect of assimilation may be enhanced by the presence of amphibole, as this phase is present in some of the cumulates (Neumann *et al.* 1999). The solidus depression expected by the release of volatiles from kaersutite breakdown potentially intensifies the anatexis of cumulate rock. Because volatile release from kaersutite is not accounted for in the model, the EC-RAFC modelling represents a minimum estimate of the mass of recycled cumulate or, alternatively, a maximum estimate of the heat exchange required to produce a certain amount of M_a. The release of partial melts from the cumulate may thus be stronger than what the model yields or, in nature, less ΔT may be required to produce a similar amount of anatectic melt. The presence of kaersutite in the cumulate rock thus supports a scenario that is prone to cannibalization of previously formed cumulate rock.

Overall, the results highlight the importance of auto-recycling at depth in ocean islands (see Harris *et al.* 2000). Notably, a similar mechanism has been suggested for basalts emitted from Piton de la Fournaise, Réunion (Salaün *et al.* 2010), as well as for other islands of the Canaries (e.g. Gurenko *et al.* 2010). Several basalt members from the Réunion eruptive phase of 1998 show enrichment of both compatible and incompatible trace elements, which has been interpreted as cannibalism of previously emplaced intrusive rock bodies (i.e. magma–wallrock interaction). O'Hara (1998) iteratively modelled an ocean island plumbing

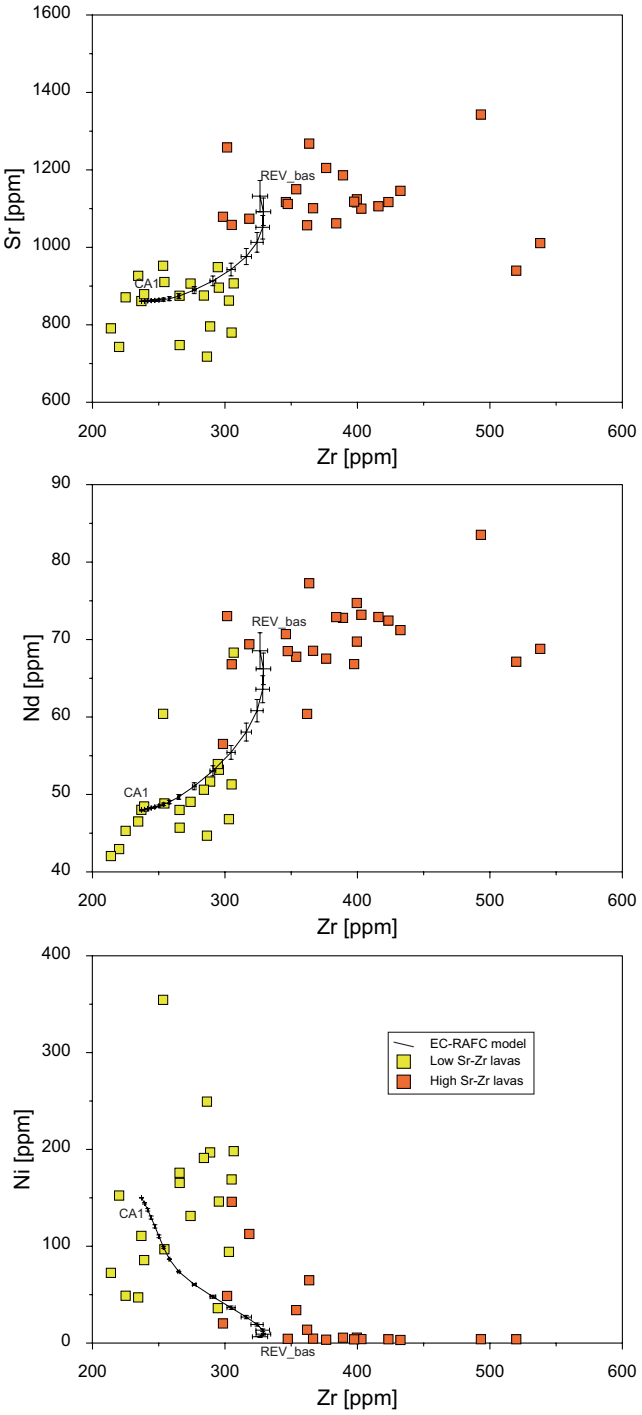

Fig. 8. Natural data of mafic Teide lavas compared with Zr, Sr, Nd and Ni concentrations modelled with the EC-RAFC code. Squares are natural data and lines are model results. For each iteration of the EC-RAFC code, error bars are given.

system from its 'birth' to eventual subaerial emplacement of lavas and found that the consumption of wall-rock or formerly produced cumulate is an essential factor in the evolution of a plumbing system. Auto-assimilation of previously fractionated mineral phases will strongly increase concentrations of incompatible trace elements in primitive lavas, which can be confirmed on the basis of the models calculated in this study. The EC-RAFC

model presented demonstrates the potential of auto-assimilation of previously generated cumulate to enrich Sr and Zr simultaneously, while being consistent with naturally observed concentrations of REE and compatible elements. This result testifies to the difficulty of interpreting mafic ocean island rocks as representative of primitive compositions directly derived from the mantle.

Conclusions

We employed newly available microanalytical data and pre-eruptive melt compositions that were modelled using the empirical equations of Blundy & Wood (1991), Bindeman *et al.* (1998) and Bédard (2006) to test the closed-system model for Teide–Pico Viejo. The results narrow down the thermal history of Teide mafic magmas and determine that the two broad groups of compositionally diverse mafic magmas are probably not related by closed-system crystal fractionation. Using the given constraints in an EC-RAFC model (Spera & Bohrson 2004, and references therein), which places the geochemical and model data into a thermodynamically constrained framework, the two types of mafic magma are better modelled by open-system processes. The two groups of magma probably reflect different stages of evolution and are thus snapshots of distinct stages of progressive assimilation and fractional crystallization. The high Sr–Zr group experienced AFC-style cumulate recycling within one or multiple magma chambers during extended periods of residence, whereas the low Sr–Zr group is less evolved and is probably the main replenishing magma at depth as it escaped voluminous cumulate recycling and thus resided for short periods in deep magma chambers.

J. Bédard and an anonymous reviewer are greatly thanked for thorough help on the manuscript and T. Rooney for the thoughtful editorial handling. T. Kunzmann is thanked for constructive comments on Excel-based least-squares calculation. S.W. and V.R.T. acknowledge funding from the School of Natural Sciences, Trinity College Dublin (TCD), Science Foundation Ireland (SFI), the Royal Swedish Academy of Sciences (KVA) and Uppsala University (UU).

References

Ablay, G.J. 1997. *Evolution of the Teide–Pico Viejo volcanic complex and magmatic system, Tenerife, Canary Islands*. PhD thesis, University of Bristol.

Ablay, G.J., Carroll, M.R., Palmer, M.R., Martí, J. & Sparks, R.S.J. 1998. Basanite–phonolite lineages of the Teide–Pico Viejo volcanic complex, Tenerife, Canary Islands. *Journal of Petrology*, **39**, 905–936.

Adam, J. & Green, T. 2006. Trace element partitioning between mica- and amphibole-bearing garnet lherzolite and hydrous basanitic melt: 1. Experimental results and the investigation of controls on partitioning behaviour. *Contributions to Mineralogy and Petrology*, **152**, 1–17.

Albert-Beltrán, J.F., Araña, V., Diez, J.L. & Valentin, A. 1990. Physical–chemical conditions of the Teide volcanic system (Tenerife, Canary Islands). *Journal of Volcanology and Geothermal Research*, **43**, 321–332.

Araña, V., Barberi, F. & Ferrara, G. 1989. El complejo volcánico del Teide–Pico Viejo. *In*: Araña, V. & Coello, J. (eds) *Los Volcanes y La Caldera del Parque Nacional del Teide (Tenerife, Islas Canarias)*. ICONA, Madrid, 269–298.

Araña, V., Martí, J., Aparicio, A., García-Cacho, L. & García-García, R. 1994. Magma mixing in alkaline magmas: An example from Tenerife, Canary Islands. *Lithos*, **32**, 1–19.

Bédard, J.H. 2006. Trace element partitioning in plagioclase feldspar. *Geochimica et Cosmochimica Acta*, **70**, 3717–3742.

Bindeman, I.N. & Bailey, J.C. 1999. Trace elements in anorthite megacrysts from the Kurile Island Arc: A window to across-arc geochemical variations in magma compositions. *Earth and Planetary Science Letters*, **169**, 209–226.

Bindeman, I.N., Davis, A.M. & Drake, M.J. 1998. Ion microprobe study of plagioclase–basalt partition experiments at natural concentration levels of trace elements. *Geochimica et Cosmochimica Acta*, **62**, 1175–1193.

Blundy, J.D. & Wood, B. 1991. Crystal-chemical controls on the partitioning of Sr and Ba between plagioclase feldspar, silicate melts, and hydrothermal solutions. *Geochimica et Cosmochimica Acta*, **55**, 193–209.

Bohrson, W.A. & Spera, F.J. 2001. Energy-constrained open-system magmatic processes II: application of energy-constrained assimilation–fractional crystallization (EC-AFC) model to magmatic systems. *Journal of Petrology*, **42**, 1019–1041.

Bohrson, W.A. & Spera, F.J. 2003. Energy-constrained open-system magmatic processes IV: geochemical, thermal and mass consequences of energy-constrained recharge, assimilation and fractional crystallization (EC-RAFC). *Geochemistry, Geophysics, Geosystems*, **4**, 8002, http://dx.doi.org/10.1029/20029C000316.

Borghini, G., Fumagalli, P. & Rampone, E. 2009. The stability of plagioclase in the upper mantle: subsolidus experiments on fertile and depleted lherzolite. *Journal of Petrology*, **51**, 229–254.

Carracedo, J.C. 1994. The Canary Islands: An example of structural control on the growth of large oceanic-island volcanoes. *Journal of Volcanology and Geothermal Research*, **60**, 225–241.

Carracedo, J.C. 1996. Morphological and structural evolution of the western Canary Islands: hotspot-induced three-armed rifts or regional tectonic trends? *Journal of Volcanology and Geothermal Research*, **72**, 151–162.

Carracedo, J.C. 1999. Growth, structure, instability and collapse of Canarian volcanoes and comparisons with Hawaiian volcanoes. *Journal of Volcanology and Geothermal Research*, **94**, 1–19.

Carracedo, J.C., Rodríguez Badiola, E., *et al.* 2007. Eruptive and structural history of Teide volcano and rift zones of Tenerife, Canary Islands. *Geological Society of America Bulletin*, **119**, 1027–1051.

Carracedo, J.C., Guillou, H., *et al.* 2011. Evolution of ocean-island rifts: the northeast rift zone of Tenerife, Canary Islands. *Geological Society of America Bulletin*, **123**, 562–584.

Davidson, J.P. & Bohrson, W.A. 1998. Shallow-Level Processes in Ocean-island Magmatism: Editorial. *Journal of Petrology*, **39**, 799–801.

Donoghue, E., Troll, V.R., Harris, C., O'Halloran, A., Walter, T.R. & Pérez Torrado, F.J. 2008. Low-temperature hydrothermal alteration of intra-caldera tuffs, Miocene Tejeda caldera, Gran Canaria, Canary Islands. *Journal of Volcanology and Geothermal Research*, **176**, 551–564.

Ewart, A. & Griffin, W.L. 1994. Application of proton-microprobe data to trace-element partitioning in volcanic rocks. *Chemical Geology*, **117**, 251–284.

Fowler, S.J., Bohrson, W.A. & Spera, F.J. 2004. Magmatic evolution of the Skye igneous centre, western Scotland: modelling of assimilation, recharge and fractional crystallization. *Journal of Petrology*, **45**, 2481–2505.

Fujimaki, H. 1986. Partition coefficients of Hf, Zr, and REE between zircon, apatite, and liquid. *Contributions to Mineralogy and Petrology*, **94**, 42–45.

Galipp, K., Klügel, A. & Hansteen, T.H. 2006. Changing depths of magma fractionation and stagnation during the evolution of an oceanic island volcano: La Palma (Canary Islands). *Journal of Volcanology and Geothermal Research*, **155**, 285–306.

Gurenko, A., Bindeman, I. & Chaussidon, M. 2010. Oxygen isotope heterogeneity of the mantle beneath the Canary Islands: insights from olivine phenocrysts. *Contributions to Mineralogy and Petrology*, **162**, 349–363.

Hansteen, T.H., Klügel, A. & Schmincke, H.-U. 1998. Multi-stage magma ascent beneath the Canary Islands: Evidence from fluid inclusions. *Contributions to Mineralogy and Petrology*, **132**, 48–64.

Harris, C., Smith, H.S. & le Roex, A.P. 2000. Oxygen isotope composition of phenocrysts from Tristan da Cunha and Gough Island lavas: variation with fractional crystallization and evidence for assimilation. *Contributions to Mineralogy and Petrology*, **138**, 164–175.

Klügel, A., Hoernle, K.A., Schmincke, H.-U. & White, J.D.L. 2000. The chemically zoned 1949 eruption on La Palma (Canary Islands): petrologic evolution and magma supply dynamics of a rift zone eruption. *Journal of Geophysical Research*, **105**, 5997–6016.

Klügel, A., Hansteen, T.H. & Galipp, K. 2005. Magma storage and underplating beneath Cumbre Vieja volcano, La Palma (Canary Islands). *Earth and Planetary Science Letters*, **236**, 211–226.

Longpré, M.-A., Troll, V.R. & Hansteen, T.H. 2008. Upper mantle magma storage and transport under a Canarian shield-volcano, Teno, Tenerife (Spain). *Journal of Geophysical Research*, **113**, B08203.

López, C., Blanco, M.J., *et al.* 2012. Monitoring the volcanic unrest of El Hierro (Canary Islands) before the onset of the 2011-2012 submarine eruption. *Geophysical Research Letters*, **39**, L13303, http://dx.doi.org/10.1029/2012GL051846.

Márquez, A., López, I., Herrera, R., Martín-González, F., Izquierdo, T. & Carreño, F. 2008. Spreading and potential instability of Teide volcano, Tenerife, Canary Islands. *Geophysical Research Letters*, **35**. L05305, http://dx.doi.org/10.1029/2007GL032625.

Martí, J., Mitjavila, J. & Araña, V. 1994. Stratigraphy, structure and geochronology of the Las Cañadas caldera (Tenerife, Canary Islands). *Geological Magazine*, **131**, 715–727.

Martí, J., Hurlimann, M., Ablay, G.J. & Gudmundsson, A. 1997. Vertical and lateral collapses on Tenerife (Canary Islands) and other volcanic ocean islands. *Geology*, **25**, 879–882.

Morse, S.A. 1984. Cation diffusion in plagioclase feldspar. *Science*, **225**, 504–505.

NAMUR, O., CHARLIER, B., TOPLIS, M. & VANDER AUWERA, J. 2012. Prediction of plagioclase–melt equilibria in anhydrous silicate melts at 1-atm. *Contributions to Mineralogy and Petrology*, **163**, 133–150.

NEUMANN, E.R., WULFF-PEDERSEN, E., SIMONSEN, S.L., PEARSON, N.J., MARTI, J. & MITJAVILA, J. 1999. Evidence for fractional crystallization of periodically refilled magma chambers in Tenerife, Canary Islands. *Journal of Petrology*, **40**, 1089–1123.

NEUMANN, E.R., SORENSEN, V.B., SIMONSEN, S.L. & JOHNSEN, K. 2000. Gabbroic xenoliths from La Palma, Tenerife and Lanzarote, Canary Islands: Evidence for reactions between mafic alkaline Canary Islands melts and old oceanic crust. *Journal of Volcanology and Geothermal Research*, **103**, 313–342.

NIELSEN, R.L. 1992. BIGD.FOR: a FORTRAN program to calculate trace-element partition coefficients for natural mafic and intermediate composition magmas. *Computers and Geosciences*, **18**, 773–788.

O'HARA, M.J. 1998. Volcanic plumbing and the space problem—thermal and geochemical consequences of large-scale assimilation in ocean island development. *Journal of Petrology*, **39**, 1077–1089.

OLIN, P. & WOLFF, J. 2010. Rare earth and high field strength element partitioning between iron-rich clinopyroxenes and felsic liquids. *Contributions to Mineralogy and Petrology*, **160**, 761–775.

REINERS, P.W., NELSON, B.K. & GHIORSO, M.S. 1995. Assimilation of felsic crust by basaltic magma: thermal limits and extents of crustal contamination of mantle-derived magmas. *Geology*, **23**, 563–566.

RIDLEY, W.I. 1970. The petrology of the Las Canadas volcanoes, Tenerife, Canary islands. *Contributions to Mineralogy and Petrology*, **26**, 124–160.

RODRÍGUEZ-BADIOLA, E., PÉREZ-TORRADO, F.J., CARRACEDO, J.C. & GUILLOU, H. 2006. Petrografía y geoquímica del edificio volcánico Teide–Pico Viejo y las dorsales noreste y noroeste de Tenerife. *In*: CARRACEDO, J.C. (ed.) *Los volcanes del Parque Nacional del Teide/El Teide, Pico Viejo y las dorsales activas de Tenerife*. Organismo Autónomo Parques Nacionales Ministerio de Medio Ambiente, Madrid, 129–186.

SALAÜN, A., VILLEMANT, B., SEMET, M.P. & STAUDACHER, T. 2010. Cannibalism of olivine-rich cumulate xenoliths during the 1998 eruption of Piton de la Fournaise (La Réunion hotspot): implications for the generation of magma diversity. *Journal of Volcanology and Geothermal Research*, **198**, 187–204.

SPERA, F.J. & BOHRSON, W.A. 2001. Energy-constrained open-system magmatic processes I: general model and energy-constrained assimilation and fractional crystallization (EC-AFC) formulation. *Journal of Petrology*, **42**, 999–1018.

SPERA, F.J. & BOHRSON, W.A. 2002. Energy-constrained open-system magmatic processes 3. Energy-constrained recharge, assimilation, and fractional crystallization (EC-RAFC). *Geochemistry, Geophysics, Geosystems*, **3**, 8001, http://dx.doi.org/10.1029/2002GC000315.

SPERA, F.J. & BOHRSON, W.A. 2004. Open-system magma chamber evolution: an energy-constrained geochemical model incorporating the effects of concurrent eruption, recharge, variable assimilation and fractional crystallization (EC-E'RAχFC). *Journal of Petrology*, **45**, 2459–2480.

STRONCIK, N., KLÜGEL, A. & HANSTEEN, T. 2009. The magmatic plumbing system beneath El Hierro (Canary Islands): Constraints from phenocrysts and naturally quenched basaltic glasses in submarine rocks. *Contributions to Mineralogy and Petrology*, **157**, 593–607.

TROLL, V.R., WALTER, T.R. & SCHMINCKE, H.U. 2002. Cyclic caldera collapse: piston or piecemeal subsidence? Field and experimental evidence. *Geology*, **30**, 135–138.

WATSON, E.B. & HARRISON, T.M. 1983. Zircon saturation revisited: temperature and composition effects in a variety of crustal magma types. *Earth and Planetary Science Letters*, **64**, 295–304.

WATTS, A.B. & MASSON, D.G. 1995. A giant landslide on the north flank of Tenerife, Canary Islands. *Journal of Geophysical Research*, **100**, 24487–24498.

WIESMAIER, S. 2010. Magmatic differentiation and bimodality in oceanic island settings—Implications for the petrogenesis of magma in Tenerife, Spain. PhD thesis, Trinity College Dublin.

WIESMAIER, S., DEEGAN, F., TROLL, V., CARRACEDO, J., CHADWICK, J. & CHEW, D. 2011. Magma mixing in the 1100 AD Montaña Reventada composite lava flow, Tenerife, Canary Islands: Interaction between rift zone and central volcano plumbing systems. *Contributions to Mineralogy and Petrology*, **162**, 651–669.

WIESMAIER, S., TROLL, V.R., CARRACEDO, J.C., ELLAM, R.M., BINDEMAN, I. & WOLFF, J.A. 2012. Bimodality of lavas in the Teide–Pico Viejo succession in Tenerife—the role of crustal melting in the origin of recent phonolites. *Journal of Petrology*, **53**, 2465–2495.

WOLFF, J.A. & TONEY, J.B. 1993. Trapped liquid from a nepheline syenite: a re-evaluation of Na-, Zr-, F-rich interstitial glass in a xenolith from Tenerife, Canary Islands. *Lithos*, **29**, 285–293.

ZACK, T. & BRUMM, R. 1998. Ilmenite/liquid partition coefficients of 26 trace elements determined through ilmenite/clinopyroxene partitioning in garnet pyroxene. *In*: GURNEY, J.J., GURNEY, J.L., PASCOE, M.D. & RICHARDSON, S.H. (eds) *Proceedings of the 7th International Kimberlite Conference*. Red Roof Design, Cape Town, 986–988.

Received 9 February 2012; revised typescript accepted 13 March 2013.
Scientific editing by Tyrone Rooney.